Delineating the macroscale areal organization of the macaque cortex in vivo

Ting Xu[1,2], Arnaud Falchier[1], Elinor L. Sullivan[3], Gary Linn[2], Julian Ramirez[4], Deborah Ross[2], Eric Feczko[4], Alexander Opitz[2], Jennifer Bagley[3], Darrick Sturgeon[4], Eric Earl[4], Oscar Miranda-Domingue[4], Anders Perrone[4], Cameron Craddock[1,2], Charles Schroeder[2,5,6], Stan Colcombe[2], Damien Fair[4], Michael Milham[1,2]

[1]Center for the Developing Brain, Child Mind Institute, New York, NY 10022, USA, [3]Center for Biomedical Imaging and Neuromodulation, Nathan Kline Institute for Psychiatric Research, Orangeburg, NY 10962, USA, [3]Divisions of Neuroscience and Cardiometabolic Health, Oregon National Primate Research Center, Beaverton, OR. [4]Department of Behavior Neuroscience, Department of Psychiatry, Advanced Imaging Research Center, Oregon Health & Science University, OR 97239, [5]Department of Neurological Surgery, Columbia University College of Physicians and Surgeons, New York, NY 10032, [6]Department of Psychiatry, Columbia University College of Physicians and Surgeons, New York, NY 10032.

Abstract

Complementing longstanding traditions centered around histology, functional magnetic resonance imaging approaches are rapidly maturing in their ability to delineate brain areal organization at the macroscale. In particular, automated approaches focused on the detection of gradient-based boundaries in functional connectivity (FC) properties between cortical areas have demonstrated the ability to characterize human brain organization at the individual level and recapitulate previously established cytoarchitectonic brain areas. The use of non-human primates (NHP) provides the opportunity to overcome critical barriers in the advancement of translational research. Here, we establish the data and scanning condition requirements for achieving reproducible, stable and internally valid areal parcellations at the individual levels, which have good correspondences with previously established postmortem areas; the inclusion of data from two independent imaging sites ensures the reproducibility of our findings. We demonstrate that highly reproducible areal organizations that can be used for fingerprinting can be achieved whether subjects were scanned under anesthesia or awake (rest, naturalistic viewing); though differences between awake and anesthetized states precluded the detection of individual differences across states; individual differences were notably more stable across differing awake states. Comparison of awake and anesthetized states suggested a more nuanced picture of changes in connectivity for higher order association areas, as well as visual cortex. These results establish feasibility and data requirements for the generation of reproducible individual-specific parcellations in NHP, as well provide insights into the impact of scan state on findings.

Introduction

The non-human primate brain model remains one of the most promising vehicles for advancing translational neuroscience (Essen, 2012; Nelson and Winslow, 2008; Phillips et al., 2014; Rilling; Vanduffel et al., 2014; Mars et al., 2011; Hutchison et al., 2015). This is particularly true for investigations requiring the definition or manipulation of cortical areas and their associated circuitry. However, lines of inquiry tend to focus on the delineation of one cortical area or circuit at a time, in part due to the reliance on histologic techniques that inherently necessitate a more targeted window of examination. Beyond their labor intensiveness, such methodologies require sacrifice of an animal to achieve the intended results, which inherently limits the longitudinal examinations needed to study neuroplasticity, neuromodulation and brain development. The availability of histological atlases for various non-human primate species provides an alternative means of guiding intracranial measurements and interventions. However, such atlases are inherently limited in their ability to account for differences in brain areal organization among animals, which can negatively impact experimentation when not properly considered (Cerliani et al., 2017; Gordon et al., 2017a, 2017b; Van Essen et al., 2016).

Recent fMRI studies in the humans imaging literature have demonstrated the feasibility of using resting state fMRI (R-fMRI) methodologies to delineate the areal organization of the cortex at the macroscale based on intrinsic brain function (Craddock et al., 2011; Wig et al., 2014; Cohen et al., 2008; Gordon et al., 2016; Glasser et al., 2016). Inspired by the postmortem architectural parcellation approaches used to differentiate spatially contiguous areas into functional units based on differences in their cytoarchitectural properties, Cohen et al. (Cohen et al., 2008) proposed a novel approach to performing areal parcellation in the human brain that measures gradients in intrinsic functional connectivity among neighboring vertices, which can in turn be used to identify transitions across distinct functional units. This approach has been extended to the full neocortex, with applications revealing functional discrete areas at group-average level that are homogenous and reproducible across studies (Glasser et al., 2016; Gordon et

al., 2017a); several of the borders have been highlighted for their correspondence to task activations and cytoarchitectonically defined areas (Gordon et al., 2017a; Wig et al., 2014); (Buckner and Yeo, 2014). Most recently, this gradient-based boundary mapping approach has been applied at the individual-level, successfully mapping full-brain gradient and transition patterns that despite commonalities appear to be individual-specific (Gordon et al., 2017a, 2017b; Laumann et al., 2015; Xu et al., 2016) and have moderate to high test-retest reliability using as little as 20 minutes of data.

Work by several groups has suggested the possibility of parcellating the macaque brain in -vivo as well, using methods such as functional MRI, diffusion tractography and invasive neural recordings. However, to date, these studies (Neubert et al., 2015; Schönwiesner et al., 2014; Vanduffel et al., 2014; Mars et al., 2011) have primarily focused on more limited sections of cortex, e.g visual cortex, including occipitotemporal, parietal and frontal cortex. The logical extension of this work – fMRI-based parcellation of the neocortex of the macaque in its entirety – would be extremely valuable in evaluating the strengths and limitations of the macaque as a translational model (Hutchison and Everling, 2012, 2014; Hutchison et al., 2012a, 2012b; Miranda-Dominguez et al., 2014; Shen et al., 2012).

In the present work, we pursue this aim using gradient-based fMRI parcellation methods to arrive at a putative map of the areal organization of the macaque cortex in its entirety. Although promising based on the human literature, there are several challenges that need to be addressed to achieve this goal, namely, 1) the feasibility of the boundary mapping parcellation in an individual macaque; 2) the validity of the parcellation; 2) the reliability of the gradient-based boundary mapping approach across scans in an individual macaque; and 3) the stability of the parcellation and the quantity of individual data required for an accurate estimate of full-brain functional areal organization. To address these challenges, we made use of four adult rhesus macaque datasets from two independent research institutions the Nathan Kline Institute (NKI-Dataset; n=2) and Oregon Health and Science University (OHSU-Dataset; n=2). Each macaque dataset includes between 184 and 728 min of awake and/or anesthesized fMRI scans. Using

these data, we first identified the individual-specific functional boundaries (i.e. edge density) and areal parcellation for each dataset and compared it against the available anatomical borders from previous studies. Then, we assessed the functional homogeneity of the gradient-based areal parcellation and demonstrated the uniqueness of the result obtained for each specific monkey. We also evaluated the stability of functional connectivity (FC) profiles, gradient and boundary maps to investigate the total quantity of data required for estimate full-brain functional areal organization. In addition, we examined the impact of monocrystalline iron oxide ferumoxytol (MION) contrast on data needs for parcellation, as prior work has demonstrated its utility in increasing the ability to detect functional connectivity patterns for non-human primates, when scanning at 3.0T (Grayson et al., 2016); similarly, we examined the potential influences of anesthesia, which is known to decrease measures of FC somewhat (Hutchison et al., 2014). Together, these analyses establish feasibility and data requirements for the generation of reproducible individual-specific parcellations in the non-human primate, as well provide insights into the impact of varying factors (e.g., scan state) on findings.

Results

High Reproducibility of Gradient-based Parcellations

For each of the macaques, the gradient, edge density and corresponding parcellations were first calculated using awake fMRI data with MION contrast (see Supplemental Information for the details), collected from the same macaques at the NKI site. The gradient evaluates the spatial transitions in the similarity of neighboring FC profiles across the native cortical surface. Corresponding edges and parcels across animals were identified from the gradient maps using the ‘watershed’ algorithm (Gordon et al., 2016). The details of this methods were described in previous studies (Laumann et al., 2015; Xu et al., 2016). Of note, the awake fMRI data were acquired with naturalistic viewing paradigm – movies were playing during the awake scans for NKI dataset. To investigate the impact of awake states (movie and rest), we additionally collected one

pure rest session for one animal. In the following session, ‘awake’ states without any specification in this results session were naturalistic viewing states.

In the awake states with MION contrast, within animal, the gradients and edge density detected by this method demonstrated high reproducibility across individual scans (see Supplement Figure S1). Consistent with prior work in humans, gradient maps showed a higher degree of reproducibility than edge maps when equivalent amount of data were used. In order to obtain a better assessment of the upper bound for reproducibility, we randomly divided the scans for each macaque into two subsets (i.e., split halves) and regenerated gradient and edge maps for the data available in each subset. Over 1,000 randomizations, markedly higher reproducibility was shown for each of the measures, as well as the resultant parcellation maps (Figure 1). The spatial correlations between two gradient maps for macaque NKI-R and NKI-W while awake were 0.79 and 0.92; for edge density, the correlations were 0.42 and 0.71. The Dice coefficient between two parcellations were 0.69 and 0.76.

Next we looked at data obtained during the anesthetized state using MION in subjects from each site, NKI and OHSU. Similar with the awake results, we observed a high degree of reproducibility in gradients, edge density and corresponding parcellations. The spatial correlations in gradients between subsets were 0.96 (NKI-R), 0.87 (NKI-W), 0.92 (OHSU-1), and 0.87 (OHSU-2); for the edge density were 0.60, 0.48, 0.65 and 0.56. The Dice coefficient between parcellations were 0.69, 0.74, 0.70, and 0.67.
In addition, we examined the reproducibility of gradient, edge density and parcellations using data obtained without MION. Compared with the data using MION, the findings were similar but less reproducible. Specifically, in the awake states from NKI dataset, the spatial correlations between two subsets were 0.48 and 0.76 in gradients, 0.24 and 0.53 in edge density, 0.67 and 0.72 in parcellations. In the anesthetized data from OHSU, the spatial correlations were 0.64 and 0.60 in gradients, and 0.53 and 0.38 in edge density. The Dice coefficient were 0.70 and 0.67 for the final parcellations.

Comparison of Parcellation with Known Topographic Areas

To further assess the validity of the parcellation maps using an external reference, the putative boundaries delineated by our functional gradient-based parcellation was overlaid with the areas 3, 4, and 17 borders previously established using post-mortem histology (Brodmann 1905). As depicted in Figure 2, the parcels derived by gradient-based mapping were approximates overlapped with areas 3, 4, and 17 borders. This suggests that gradient-based boundaries represent differences in function within a topographically organized area that are captured by histologic and topographic mapping. It is important to note that while there were clear correspondences between our findings and those of the postmortem map obtained from prior work, some notable differences exist. While such differences may suggest greater detectability, or the detection of a unique aspect of the functional architecture in the macaque, the possibility of artifactual findings related to the imaging also need to be considered. For example, in early visual cortices (e.g., the fractionates in area 17), we found additional edges not apparent in the postmortem map; examination of the raw data for these divisions suggests they may reflect an artifact arising from incomplete coverage, though alternatively, they may reflect the presence of further subdivisions. Future work with optimized imaging will be required to help differentiate between these possibilities.

Parcellation Homogeneity

Consistent with prior work in humans, we assessed the internal validity of the parcellation maps obtained for each macaque. Specifically, we calculated the homogeneity of FC similarity in the parcels generated from subset 2 (reference subset) using the data from subset 1 (test subset). The mean homogeneity across all parcels and two macaques in awake with MION condition was 0.88, while under anesthesia across four macaques was 0.84 (Figure 3, red line). Then, we assessed the degree to which this parcellation was more homogenous than a null distribution of mean homogeneities generated from 1000 ‘random’ parcellation maps for the same subject; each of these maps were generated by randomly rotating the parcellation units around the cortical surface for each subject (Gordon et al., 2016). The mean homogeneity of null model parcellations was no more than 0.75 for four macaques (these findings are

comparable to those previously reported in humans (Laumann et al., 2015; Xu et al., 2016); in each macaque, the real parcellations were significantly greater than that obtained in null model parcellations (awake: Z score = 6.74, 5.04, $p<0.001$; anesthesia: 10.98, 5.11, 8.50, 5.93, $p<0.001$, Figure 3).

Additionally, we compared the homogeneity across different states (awake vs. anesthesia) and contrast types (MION vs. NO-MION). To facilitate a relatively fair comparison between states within each subject, we subsampled the reference and test subset to the same amount of time. The MION data exhibited higher homogeneity than NO-MION condition regardless of awake (Figure 4, blue line) or anesthetized states (Figure 4, turquoise line). These differences between awake and anesthesia are examined and discussed in the later sections.

Data Requirements for mapping the reliable FC, gradient and edges

A key challenge for imaging efforts focused on brain parcellation is the determination of minimal data requirements to reliably and consistently capture individual parcellations. While the human imaging literature is actively working to establish data requirements, functional MRI imaging in non-human primates faces additional challenges. In particular, decreased signal to noise characteristics relative to humans due to smaller voxels size required, and the usage of anesthetics. The iron-based contrast agent, MION, is increasingly being used to overcome these challenges, particularly when scanning at 3.0T (Gautama et al., 2003; Grayson et al., 2016; Leite et al., 2002); however, the necessity of MION, particularly in the awake macaque, is not clear.

Here, we first examined the stability of gradient and edge maps derived from data obtained during the awake state using MION in the NKI-dataset. More specifically, for each of the two macaques imaged in the awake state, we randomly split the data obtained with MION into two independent subsets (120 minutes for each subject NKI-W ; 44 minutes each for NKI-R) and used subset 2 to derive reference FC, gradients and edge density. Next, we randomly sampled subset 1, started at 8-minute amount, adding in six 4-min increments, followed by three 8-minute increments of data, and then (for subject NKI-W only) two 16 minute increments (i.e. 8, 12, 16, 20, 24, 28, 32, 40, 48, 56,

72, 88 min); the maps generated from each increment were compared to the reference maps in the same macaque. The results convergent estimation for FC are averaged from 1,000 random samplings of data at each time point. Of note, to facilitate the computational capacity for gradient and edge density calculation, the results of gradient and edge density were calculated on the down-resampled 400 regions of interest vertices for 100 times at each time point.

Consistent with prior human work, the average FC, gradients and edge density from awake state (Figure 5, green line) were progressively increased by the amount of data incorporated into the analysis. Focus on the subject NKI-W who has more data, the average similarity (i.e. correlation) of 8 min from subset 1 with subset 2 (reference) was 0.74 (SD=0.04) for FC, 0.76 (SD=0.05) for gradient and 0.39 (SD=0.04) for edge density. The correlations were rapidly increased to 0.94 (SD=0.008) for FC, 0.86 (SD=0.032) for gradients with 28 min of data, and 0.60 (SD=0.028) for edge density with 40 min of data. The averaged similarity were then slowly increase to 0.97 (SD=0.002) for FC, r=0.90 (SD=0.008) for gradients and 0.66 (SD=0.011) for edge density with 88 min of data. Similar results were found in subject NKI-R while the overall similarities were lower than subject NKI-W as less data was collected.

Next we looked at data obtained during the anesthetized state using MION in subjects from each site, NKI and OHSU. Again, we compared findings obtained using two distinct subsets of data in each subject finding a stability profile highly similar to that observed in the awake state (Figure 5, red line). For each of the monkeys, the parcel-based FC, gradient and corresponding edge density uninterruptedly increased from 8 min to 28 min and began to plateau after 40~56 min. At the 8 min point, the average correlations across four monkey from subset 1 with subset 2 (reference) were only 0.81 (SD=0.06) for FC, 0.66 (SD=0.08) for gradient, and 0.28 (SD=0.05) for edge density, while increased to 0.92 (SD=0.02) for FC, 0.84 (SD=0.04) for gradient, and 0.44 (SD=0.09) for edge density at 40 min. The similarity is increased to 0.93 (SD=0.003) for FC, 0.89 (SD=0.03) for gradient, and 0.59 (SD=0.05) for edge density at 110 min in the OHSU dataset.

In order to establish the impact of MION, for each of the four macaques, we also examined the stability of FC, gradient, edge density generated using the data obtained without MION (Figure 5, awake: blue line, anesthesia: turquoise line). When the data obtained for each monkey without the use of MION was divided into two subsets, the correspondence remains notably lower than obtained with MION - regardless of whether anesthesia was used (OHSU-1, OHSU-2) or not (NKI-W, NK-R).

Identification of unique individual areal boundaries (fingerprinting)

Next, we worked to confirm that despite apparent commonalities, the parcellations obtained were unique to each individual. To accomplish this, we assessed the similarity of the gradients and edge density generated across the four macaques and subsets (i.e. subset 1 and subset 2 for each macaque); Figure 6 depicts the spatial correlation between 20 gradient maps (2 macaque x 2 subsets x 3 conditions from NKI and 2 macaques x 2 subsets x 2 conditions from OHSU), as well as between 20 edge density maps (Figure 6). The correlations between subsets within a given subject in the same state (awake or anesthetized), are notably greater than those between different subjects. When looking within the same state, an individual can be successfully identified from others using half of dataset for each macaque. Of note, the correlations in gradient and edge density across the monkey while under anesthesia (cadet blue dots) is higher than while awake (turquoise dots) - possibly suggesting that functional boundaries are more prone to variation while awake. Across states, measures obtained from data in the same macaque under two different awake states (i.e., naturalistic viewing, rest exhibited a relatively high degree of similarity (fuchsia dots). However, the correlations in findings between awake and anesthetized (yellow dots) states in the same macaque were much less than those obtained in the same state. In addition, we also observed site effects, with correlations between monkeys across two sites (purple dots) being lower than within the same site while under same circumstance (Anesthesia with MION).

Effect of MION

As can be seen in Figure S1, compared to the MION data within the same macaque, the FC, gradient and edge density maps obtained without MION have a relatively modest correspondence with those obtained using MION in anesthesia data (dark green dots). Similar but relatively lower correspondences were observed in the awake data from NKI-dataset (light green dots). These findings suggest that the signal obtained with MION is notably improved relatively to standard BOLD fMRI.

Effect of State During Awake Imaging

Here, we examined the impact of differences among awake states by comparing functional connectivity, gradient and edge maps produced during the viewing of movies with those obtained during rest. Human imaging studies have drawn attention to the overall stability of functional connectivity patterns across differing awake conditions, despite more fine-grained modifications in connectivity associated with manipulations of state (e.g., rest, movies, task performance). Consistent with the findings from humans, we found a high degree of similarity between functional connectivity patterns (r=0.79) associated with rest and those observed with movie viewing. At the network level, a similar connection profile was found within and between networks except lateral visual, which showed greater within network connectivity in movie viewing than rest. Regarding the gradient and edge density, we also found a relatively high similarity for each, the gradient maps and the parcellation maps generated using the two awaken states (movie and rest). The spatial correlation of gradient was 0.59 and Dice coefficient of parcellations was 0.68. As the similarity of FC, gradient and edge density between two awake states (movie and rest) within each monkey (see Figure 6 fuchsia dots) is higher than across monkeys in the awake movie state, this suggests that naturalistic viewing, which is more favorably tolerated by non-human primates, can be used for the fingerprint.

Effect of Anesthesia

As reported in the prior section, the FC, gradient and edge density generated from differing subsets of data obtained with anesthesia showed a high degree of correspondence, similar to what was observed when subsets of data collected while

awake were compared. However, the correspondence of areal organization measures was substantially lower when compared across the awake and anesthetized states in the same subjects (NKI-R, NKI-W). Specifically, compared to the awake condition, the spatial correlations in FC between awake and anesthesia was 0.52 (SD=0.08) (Figure 6A, yellow dots). The gradient and edge density showed even less similarity between awake and anesthetized, with the spatial correlations across states with half subsets of data in NKI-dataset being 0.25 (SD=0.14) and 0.12 (SD=0.02) respectively (Figure 6B-C, yellow dots).

The lower correspondence of findings between states (awake, anesthetized) relative to within a state was not necessarily surprising. Previous studies have suggested that the spatial and temporal properties of functional connectivity observed in non-human primates can be impacted by anesthesia, with the profundity of the efforts observed depending on the depth of anesthesia (Hutchison et al., 2012; 2013; Vincent 2007). Visual examination of the FC matrices for the awake states (rest, movies) and anesthesia revealed notable regional connectivity differences that appeared to be specific to anesthesia (Figure 7B). To facilitate detection of those connections with the greatest change, for each monkey, we: 1) calculated the difference score (FC[awake] - FC[anesthesia]) for each connection, and then 2) transformed them to Z-scores based upon the mean and standard deviation for difference scores throughout the brain (Figure 7C). To make network-specific statistical inferences, for each network, we compared FC across each set of connections within the network using a paired t-test; to provide conservative estimates that avoid inflation based on the number of connections, significance was estimated by randomization (10,000 times) for a given pairing of networks. The same procedure was carried out to look at connections between pairings of networks. False discovery rate was used to correct for multiple comparisons (Figure 7D).

Consistent with prior work, we found evidence of anesthesia-related decreases within and between most networks, with specific findings differing somewhat between the two monkeys. Decreases in within-network FC for the dorsal salience, dorsal motor, lateral

visual, and medial visual networks were consistent across the two subjects. Of note, although more limited, there was also evidence of anesthesia-related increases in FC - most notably in the posterior cingulate cortex default mode network (PCC-DMN) for the two subjects. Complementing these within-network findings were anesthesia-related increases in between network FC for the visual networks; these increases were most consistent for FC with default network and fronto-parietal components. Of note, while comparison of awake and anesthetized states was not possible for the datasets collected at OHSU, the sparsity of the data collected there was more similar to that obtained under anesthesia at NKI, suggesting some level of consistency.

Discussion

The present work assessed the ability of a gradient-based FC boundary mapping approach to map the areal organization of the non-human primate brain at the individual level and yield reproducible results. In particular, the present work demonstrated the ability to move beyond network- and region-specific parcellations, to provide full cortical parcellations. Importantly, we found that: 1) areal boundaries are highly reproducible in individual macaques, though substantial amounts of data are required, 2) resultant parcellations appear to exhibit construct validity per homogeneity analyses and comparison to parcellations obtained from diffusion imaging and morphometry, 3) functional connectivity patterns, and their resultant gradients and edge maps appear to be stable across waken states, though markedly different across awake and anesthetized states, 4) enhancement of non-human primate imaging using MION appeared to be essential for obtaining reasonable signal stability in a reasonable time period, 5) similar to humans, despite gross similarities, individual-specific functional connectivity and parcellation patterns were readily detectable per fingerprinting analyses, 6) alignment of nonhuman and human parcellation results into a common space gives rise to the potential for enhancing trans-species studies.

Gradient-based areal boundaries area highly reproducible in individual macaques with sufficient data

Our findings regarding reproducibility and data requirements are not surprising given recent work carried out in humans. (Gordon et al., 2017a; Laumann et al., 2015; Xu et al., 2016). Similar to the findings from humans, more data is generally better when addressing the reproducible FC (Laumann et al., 2015), though with the largest gains being observed as the data used increases up to ~32 min - a finding that echoes the findings from humans, where the most substantial gains were seen up to around 27-30 minutes. It should be noted that the data needs increase with each additional step of processing (i.e., FC->gradient->edge maps). Improvements in reliability for gradients and parcellation slowly but continuously increased as data increased to 40 min, while the largest reproducibility values (spatial correlation and Dice coefficient) were still relatively lower than what can be achieved for FC. These findings suggest that extended data are required to achieve a similar level of reproducibility of parcellations. Additionally, our findings extend recent works emphasizing the importance of contrast agents when scanning non-human primates at 3.0T by demonstrating that the use of MION is a prerequisite to achieving maximal reproducibility for FC, gradients, and functional boundaries maps (Gautama et al., 2003; Grayson et al., 2016; Leite et al., 2002); this is true regardless of whether anesthesia was used or not.

The gradient-based parcellation show internal validity

Directly relevant to the present study, prior studies in humans suggest that the boundary map-based parcellation had highly homogeneous FC patterns at the group and individual level (Gordon et al., 2017a; Laumann et al., 2015; Xu et al., 2016). In the current study, we tested the homogeneity of boundary map-derived parcellations using 50 percent subsets of the data (subset 1), such that the parcels were generated completely independently from the other half of the dataset (subset 2) for each status within each macaque. On average, the parcel homogeneity was above 0.9 with 120 min of awake data. This high degree of homogeneity indicates that most parcels represented regions of similar functional connectivity pattern. It is notable that the homogeneity varied across parcels. As discussed in a previous study (Gordon et al., 2016), the homogeneity of parcels is associated with parcel size, where small parcels

are more likely to have higher homogeneity than larger parcels. A few parcels had low homogeneity and some of them, e.g. in the frontal pole, anterior inferior temporal lobe, may be caused by the low-SNR or distortion signal in those areas. Accordingly, it is necessary to use a null model to truly evaluate the homogeneity. By creating the null model from 1000 randomly rotating of the identical parcellations around the cortical surface, we found that the homogeneities of parcels were significantly higher than the null model in both awake and anesthetized states. Consistent with the finding in the human literature (Gordon et al., 2016); (Laumann et al., 2015), this suggested that the overall gradient-based parcellations can successfully delineate the functional homogeneous cortical areas in individual macaque.

A key challenge for any effort focused on cortical parcellation, whether in the human or non-human primate, is determination of the 'correct' number of parcels. Regardless of which modality or parcellation method is used, a number of differing criteria can be used to make such determinations. In the current study, the watershed flood algorithm yielded between 110 and 140 parcels per hemisphere, for each macaque. An advantage of this methodology, is the lack of need for a priori specification of the number of parcels to be produced. However, the results can be impacted by properties of the data, such as spatial resolution and smoothness; in this regard, a priori specification of parameters (e.g., number of parcellations) can have advantages. Our estimate for number of parcels convege with current estimates generated from histology-based studies (i.e. cytoarchitecture, myeloarchitecture, and chemoarchitecture), which have increased from 78-88 (Felleman and Van Essen, 1991; Markov et al., 2010; Van Essen et al., 2012; Lewis and Van Essen, 2000) to 130-160 in each hemisphere (Paxinos and Franklin, 2004; Van Essen et al., 2012). Future work will benefit from integrative examinations across assessment modalities (e.g., functional MRI, diffusion, histology) in the same animals.

Rest and naturalistic viewing during awake imaging show similar functional properties

Our findings regarding the relative stability of functional connectivity patterns across awake and sensitivities to level of arousal (i.e., sleep, anesthesia) help to synthesize previous findings from the human and non-human primate literatures. Over the past decade, numerous studies have demonstrated the ability to extract highly similar intrinsic functional connectivity networks, regardless of whether imaging is carried out during an active task state or rest (Cole et al., 2014; Fair et al., 2007; Vanderwal et al., 2017). Recent work has increasingly highlighted the potential value of using non-rest states, particularly naturalistic viewing, for assessing functional connectivity, as head motion appears to be lower and tolerability higher. While systematic differences in connectivity patterns are undoubtedly present across states, as revealed by within subject comparisons, differences in connectivity patterns across individuals remain largely intact - at least for static functional connectivity patterns (Finn et al., 2015; O'Connor et al., 2016; Vanderwal et al., 2017; Wang et al., 2017). Given the various behavioral demands of awake imaging for non-human primate, we have found that naturalistic viewing conditions can be particularly valuable - at least for full-brain parcellations. For those interested in more fine-grained parcellations or temporal dynamics, it is important to further investigate the temporal stability vs. state-dependence of more subtle distinctions within cortical areas (e.g., polar angle and eccentricity mapping in early visual cortex).

Individual areal organization is unique while the awake and anesthetized states show distinct profiles

As suggested by prior work in humans, we found that individual areal organization in the monkey can be used for fingerprinting. Within the same condition (awake-awake, anesthesia-anesthesia), the within-individual spatial correlations of gradient and edge density maps are explicitly higher than between-individual correlations. Consistent with prior work (Finn et al., 2015; O'Connor et al., 2016; Vanderwal et al., 2017), the ability to fingerprint could be achieved across different awake conditions (i.e., movie, rest), though some decrements in similarities for FC, gradients and edge maps were noted. Importantly, the ability to fingerprint using data collected with anesthesia was notably decreased when attempting to match the same subject across the awake and

anesthetized states. This is not surprising, as the similarities for full-brain FC, gradient maps and edge maps were dramatically reduced when looking across the awake and anesthetized states (e.g., ~40% in whole-brain FC similarity).

While the presence of differences in FC properties between awake and anesthetized states was not surprising based on prior work (Hutchison et al., 2013, 2014; Vincent et al., 2007), some of the specific findings suggest a more nuanced picture than previously appreciated. Consistent with prior studies varying levels of anesthesia, we found evidence of anesthesia-related compromises in within- and between-network connectivity for higher-order associative cortices; the specific networks affected differed somewhat across the two monkeys, with the most consistent findings being observed in the salience and dorsal attention networks. However, unlike prior studies, which largely relied on variations of depth of anesthesia, our comparison of awake states and anesthesia also suggested that the visual networks and their connectivity with default and frontoparietal networks actually showed anesthesia-related increases in connectivity. Overall, these findings echo those findings of recent studies of the impact of anesthetics on brain differences in humans, which suggested a loss of complexity in the functional architecture of the brain (Vanhaudenhuyse et al., 2010; Noirhomme et al., 2010).

In sum, the present work suggests that each, the awake and the anesthetized states, as well as their differences, are highly stable. Future work would benefit from more detailed examinations of anesthesia effects that include awake imaging, as well as possibly natural sleep.

Effects of Sites

Finally, it is worth noting a unique aspect of the present work - the examination of of monkey datasets across two institutions. A significant advantage of this strategy was the ability to confirm the reproducibility of findings across two independently collected datasets. Not surprisingly, while we were successful in demonstrating the generality of our findings, we did find evidence of site-related differences. Specifically, we found that

the correspondence of gradient and edge maps among subjects was higher within a site than between. Possible factors that might explain site-related variation include differences in: 1) anesthesia protocols (e.g. the knockout agent and delay duration after the time of anesthetics administration); 2) head coils; the OHSU dataset was acquired by a knee coil while NKI dataset was with a surface coil; prior work has demonstrated differences in signal properties (including distortion) of the data obtained from monkeys using these coils (Grayson et al., 2016); 3) rearing histories. Future work would benefit from more coordinated efforts focused on multi-site imaging in the non-human primate as a means of maximizing the reproducibility of findings between laboratories.

Limitations

It is important to note that despite the various successes of the present work, a number of limitations and potential areas for future optimization exist. As previously discussed, a key limitation of any parcellation methodology is the lack of a gold standard benchmark to help establish validity. The present work made use of comparisons to previously established histologic parcellations to provide insights into validity, as well as the examination of parcel properties (i.e., homogeneity). Future work would benefit from examination of multiple methods of parcellation in the same subjects (e.g., fMRI and diffusion imaging, fMRI and myelin maps, fMRI and histology). Another consideration for future work is examination of the potential impact of preprocessing strategy decisions on the resultant parcels and their stability. Optimization of preprocessing may be particularly useful if focused on bringing down data needs for achieving the same parcellation results. Finally, the present work relied on the iFC similarity measure used in prior studies for gradient-based parcellation. Prior work demonstrated this measure to have favorable properties relative to several other possible measures. However, an exhaustive examination of measures to be used for gradient-based parcellation has yet to be carried out; this would be of benefit both - to determine if some measures may be able to lead to more fine-grained parcellations, and to find a less computationally costly measure if possible. On a related note, a range of alternatives exist for the final parcellation step in the gradient-based strategy - future work determining optimality is merited.

Conclusions and Future Directions

In summary, the present work demonstrates the ability to achieve highly reproducible, individual-specific cortical parcellations in the non-human primate. Our findings also highlight the many factors that can contribute to stability, in particular the need for sufficient data and contrast agents. Our findings also emphasized the need for consideration of state (i.e., awake vs. anesthetized) when interpreting findings and their reproducibility across studies, as well as during the study design process. Transformation of our non-human primate findings into a common space demonstrated a future direction that can be further optimized to facilitate comparative and translational studies.

METHODS

Dataset 1, NKI-Macaque

The Macaque dataset 1 consisted of 2 rhesus monkey (Macaca mulatta, 1 male, age 6 years, marked as NKI-R in the current study, 6.4 kg, 1 female, age 7 years, 4.5 kg, marked as NKI-W), which were collected from the Nathan Kline Institute for Psychiatric Research. All methods and procedures were approved by the NKI Institutional Animal Care and Use Committee (IACUC) protocol. The monkeys were previously implanted with an MRI-compatible custom built acrylic head post.

Data Acquisition

Structural MRI data were obtained with a Tesla Siemen Tim Trio scanner with a 32-channel surface coil adapted for monkey head scanning. T1-weighted anatomical images (TE=3.87 ms, TR=2500 ms, TI=1200 ms, flip angle=8 deg, 0.5 mm isotropic voxel) were collected for each macaques. The macaque was sedated with an initial dose of atropine (0.05 mg/kg IM), dexdomitor (0.02 mg/kg IM) and ketamine (8 mg/kg IM) intubated, and maintained with 0.75% isoflurane anesthesia for the duration of structural MRI procedures. Functional MRI scan were obtained using a gradient echo EPI sequence (TR=2000 ms, TE=16.6 ms, flip angle=45, 1.5x1.5x2mm voxels, 32 slices,

FOV=96 x 96 mm). Seven sessions were acquired for NKI-R (294 min in total) and 10 sessions (688 min) for NKI-W. Each session included 4-7 scans, 8-10 minutes per scan. We collected data under anesthesia and while the monkey were awake. The monocrystalline iron oxide ferumoxytol (MION) solution was injected at iron doses of 10 mg/kg IV prior to the scans for MION sessions. See Table S1 for details of the acquisition parameters for all collected datasets.

Dataset 2, OHSU-Macaque

The Macaque dataset 2 consisted of 2 male rhesus macaques (Macaca mulatta, 1 male, age 5 years, marked as OHSU-1, 8.6 kg, 1 male, age 5 years, 7.6 kg, marked as OHSU-2), which were collected from the Oregon Health and Science University. The animal procedures were in accordance with National Institutes of Health guidelines on the ethical use of animals and were approved by the Oregon National Primate Research Center (ONPRC) Institutional Animal Care and Use Committee.

Data Acquisition

Structural MRI data were obtained with a 3 Tesla Siemen Tim Trio scanner with a 15-channel knee coil adapted for monkey head scanning. T1-weighted anatomical images (TE=3.33 ms, TR=2600 ms, TI=900 ms, flip angle=8 deg, 0.5 mm isotropic voxel) were collected for each macaques. Functional MRI scan were obtained using a gradient echo EPI sequence (TR=2070 ms, TE=25 ms, flip angle=90, 1.5x1.5x1.5 mm voxels, 32 slices, FOV=96 x 96 mm). The macaque was sedated with an initial dose of ketamine (5 mg/kg) for intubation, and thereafter maintained on <1% isoflurane anesthesia during each scan session. Sixteen sessions were acquired for each monkey (30 min per session, 8 pure BOLD sessions and 8 sessions with MION). The BOLD and MION sessions were acquired at the same day; The BOLD session started at 45 min after the monkey was knocked out, followed by the MION sessions. The MION solution was injected at iron doses of 8 mg/kg IV . We collected data under anesthesia and while the monkey was awake. See Table S1 for details of the acquisition parameters for all collected datasets.

Image Preprocessing

The structural image processing included the following steps: 1) spatial noise removal by a non-local mean filtering operation (Zuo and Xing, 2011, 2014), 2) constructing an average structural volume from multiple T1-weight images, 3) brain extraction and tissue segmentation into gray matter (GM), white matter (WM) and cerebrospinal fluid (CSF); this was performed by FSL, FreeSurfer and ANTs, followed by manual editing to fix the incorrect volume, 4) reconstructing the native white matter and pial surfaces (FreeSurfer), 5) registering the native surface to a hybrid left-right template surface (Yerkes19 macaque atlas) (Donahue et al., 2016). The Yerkes19 template was created by 19 adult macaques acquired from Yerkes Primate Research Center and processed by Human Connectome Project (HCP) pipeline (Donahue et al., 2016; Glasser et al., 2013). The registered left and right hemisphere surfaces were brought into register with each other and down-sampled from 164k_fs_LR surface to a 10k_fs_LR (10,242 vertices) surface.

The functional image preprocessing included the following steps: 1) discarding the first five volumes of the time series and compressing temporal spikes (AFNI 3dDespike), 2) slice timing correction, motion correction, and field bias correction, 3) normalizing the 4D global mean intensity, 3) regressing out nuisance signal including the mean time series for WM and CSF masks, as well as the Friston-24 motion parameters [Yan et al., 2014]; Linear and quadratic trends were also regressed out from the data, 4) band-passed ($0.01 < f < 0.1$Hz) filtering the residuals to extract the low-frequency fluctuation, 5) registering image to the anatomical space and projecting onto the native middle surface, 6) spatial smoothing with 4 mm full width at half maximum along the native surface and down-sampled to 10k surface.

Quality Control Procedure

The frame-wise displacement (FD) and mean FD were calculated to quantify the head micromovements. The mean FD of the scans included in our analysis were less than 0.25 mm while awake, 0.05 mm under anesthesia. The average mean-FD were 0.11

(SD=0.05) across all the awake scans of two macaques and 0.023 (SD=0.006) across all the anesthetized scans of four macaques.

Surface-based iFC calculation and Gradient-based Parcellation

A cortical surface was reconstructed to provide an accurate representation of morphology and topology of brain for each macaque. The volumetric fMRI data was aligned to anatomical space and then projected to native middle cortical surface. Then the time series were smoothed along the high-resolution (about 164k vertices for each hemisphere) native middle surface (FWHM = 4 mm) and down resampled to a coarser (10,242 vertices for each hemisphere) template surface.

The procedures of surface-base FC calculation and gradient-based parcellation were similar as previous studies described in Laumann et al., (2015) and Xu et al., (2016). In brief, the functional connectivity (FC) map in full brain of gray matter tissue was first computed using the time course for each vertex, resulting in a (10,242 vertices x 20,484 vertices) matrix. The distributions of the resulting correlation values were standardized to the normal distribution using Fisher's r-to-z transform. A FC similarity profile was calculated for each vertex on the surface from the spatial correlation between the vertex's iFC map and the iFC map of every other vertex, resulting in a 10,242 vertices x 10,242 vertices symmetric matrix. Each column (or row) of this matrix represents the iFC similarity map for each surface vertex. The gradient (i.e., the first spatial derivative) of each iFC similarity map was computed on the native middle surface to measure the degree of the transition in iFC profile at each vertex, resulting in 10k gradient maps for each hemisphere. Then we used a 'watershed by flooding' algorithm (Gordon et al., 2014) for each of gradient maps - resulting in 10k binarized edge maps. Finally, the 10k gradient and edge maps were averaged to generate the final gradient and an edge density map. By applying the same watershed algorithm to the edge density map to yield the initial parcel maps.

Parcellation Validation

For each macaque, in order to compare the homogeneity across different condition (awake vs. anesthesia, MION vs. NOMION), the parcel homogeneity was evaluated by

Kendall' coefficient from all vertices in the parcel for each condition (Xu et al., 2016). Follow by the prior human study, the overall homogeneity of the parcellation was compared to a null model created by 1000 randomly rotating the parcellation on the cortical surface (Gordon et al., 2014).

Evaluating the Stability of iFC, gradients, and edge density

For each macaque, we randomly split the data from all sessions into halves within each condition, and use the half of subset (subset 2) to derive reference. Then, we randomly selected samples of 8, 12, 16, 20, 24, 28, 32, 40, 48, 56, 72, and 88 min (up to the half subset of sample for each macaque in each condition) from subset 1 to examine convergent estimates of FC, gradient and edges. Of note, previous study suggested that shorter sampling of contiguous data over more sessions can facilitate the convergence. Hence the subsamples of 8 to 88 min data were generated from multiple 2 min contiguous segments from the subset 1. The parcel-based FC was calculated to evaluate the areal-level cortical network and permuted 1000 times at each time point. The gradient and edge density were also calculated to examine the convergence of the parcellation. To facilitate the computational capacity for gradient and edge density calculation, the results of gradient and edge density was calculated on the down-resampled 400 regions of interest vertices for 100 times at each time point.

Network Assignment

To characterize large-scale system for parcellations created in the current study, we assigned network identity to parcels using the previously established network definition from Ghahremani (2016). The matching procedure was similar with Gordon et al., (2015). Specifically, we extracted the time series and averaged within each parcel. The averaged time series was then correlated against all other times series across the cortical surface to obtain a connectivity map. The connection were excluded if the geodesic distance between parcel centers were less than 10 mm to remove the purely local connectivity (Power et al., 2011) from spatial smoothing. After that, we thresholded and binarized the connectivity map at the top 5% of connectivity strengths. The resulted in a binarized map of regions with high connectivity to that parcels. Then we examined

the overlap of this binarized map to the binarized group ICA Z-map (Z>2.33, p<0.001) from Ghahremani and defined the best match by the Dice coefficient. Then the neighboring parcels assigned in the same network were merged to create a final network-patch.

Reference

Buckner, R.L., and Yeo, B.T.T. (2014). Borders, map clusters, and supra-areal organization in visual cortex. Neuroimage *93 Pt 2*, 292–297.

Cerliani, L., D'Arceuil, H., and Thiebaut de Schotten, M. (2017). Connectivity-based parcellation of the macaque frontal cortex, and its relation with the cytoarchitectonic distribution described in current atlases. Brain Struct. Funct. *222*, 1331–1349.

Cohen, A.L., Fair, D.A., Dosenbach, N.U.F., Miezin, F.M., Dierker, D., Van Essen, D.C., Schlaggar, B.L., and Petersen, S.E. (2008). Defining functional areas in individual human brains using resting functional connectivity MRI. Neuroimage *41*, 45–57.

Cole, M.W., Bassett, D.S., Power, J.D., Braver, T.S., and Petersen, S.E. (2014). Intrinsic and task-evoked network architectures of the human brain. Neuron *83*, 238–251.

Craddock, R.C., Cameron Craddock, R., James, G.A., Holtzheimer, P.E., Hu, X.P., and Mayberg, H.S. (2011). A whole brain fMRI atlas generated via spatially constrained spectral clustering. Hum. Brain Mapp. *33*, 1914–1928.

Donahue, C.J., Sotiropoulos, S.N., Jbabdi, S., Hernandez-Fernandez, M., Behrens, T.E., Dyrby, T.B., Coalson, T., Kennedy, H., Knoblauch, K., Van Essen, D.C., et al. (2016). Using Diffusion Tractography to Predict Cortical Connection Strength and Distance: A Quantitative Comparison with Tracers in the Monkey. J. Neurosci. *36*, 6758–6770.

Essen, D.V. (2012). Surface-based analyses of human, macaque, and chimpanzee cortical organization. J. Vis. *12*, 1377–1377.

Fair, D.A., Schlaggar, B.L., Cohen, A.L., Miezin, F.M., Dosenbach, N.U.F., Wenger, K.K., Fox, M.D., Snyder, A.Z., Raichle, M.E., and Petersen, S.E. (2007). A method for using blocked and event-related fMRI data to study “resting state” functional connectivity. Neuroimage *35*, 396–405.

Felleman, D.J., and Van Essen, D.C. (1991). Distributed hierarchical processing in the primate cerebral cortex. Cereb. Cortex *1*, 1–47.

Finn, E.S., Shen, X., Scheinost, D., Rosenberg, M.D., Huang, J., Chun, M.M., Papademetris, X., and Constable, R.T. (2015). Functional connectome fingerprinting: identifying individuals using patterns of brain connectivity. Nat. Neurosci. *18*, 1664–1671.

Gautama, T., Mandic, D.P., and Van Hulle, M.M. (2003). Signal nonlinearity in fMRI: a comparison between BOLD and MION. IEEE Trans. Med. Imaging *22*, 636–644.

Glasser, M.F., Sotiropoulos, S.N., Wilson, J.A., Coalson, T.S., Fischl, B., Andersson, J.L., Xu, J., Jbabdi, S., Webster, M., Polimeni, J.R., et al. (2013). The minimal preprocessing pipelines for the Human Connectome Project. Neuroimage *80*, 105–124.

Glasser, M.F., Coalson, T.S., Robinson, E.C., Hacker, C.D., Harwell, J., Yacoub, E., Ugurbil, K., Andersson, J., Beckmann, C.F., Jenkinson, M., et al. (2016). A multi-modal parcellation of human cerebral cortex. Nature *536*, 171–178.

Gordon, E.M., Laumann, T.O., Adeyemo, B., Huckins, J.F., Kelley, W.M., and Petersen, S.E. (2016). Generation and Evaluation of a Cortical Area Parcellation from Resting-State Correlations. Cereb. Cortex *26*, 288–303.

Gordon, E.M., Laumann, T.O., Adeyemo, B., and Petersen, S.E. (2017a). Individual Variability of the System-Level Organization of the Human Brain. Cereb. Cortex *27*, 386–399.

Gordon, E.M., Laumann, T.O., Adeyemo, B., Gilmore, A.W., Nelson, S.M., Dosenbach, N.U.F., and Petersen, S.E. (2017b). Individual-specific features of brain systems identified with resting state functional correlations. Neuroimage *146*, 918–939.

Grayson, D.S., Bliss-Moreau, E., Machado, C.J., Bennett, J., Shen, K., Grant, K.A., Fair, D.A., and Amaral, D.G. (2016). The Rhesus Monkey Connectome Predicts Disrupted Functional Networks Resulting from Pharmacogenetic Inactivation of the Amygdala. Neuron *91*, 453–466.

Hutchison, R.M., and Everling, S. (2012). Monkey in the middle: why non-human primates are needed to bridge the gap in resting-state investigations. Front. Neuroanat. *6*, 29.

Hutchison, R.M., and Everling, S. (2014). Broad intrinsic functional connectivity boundaries of the macaque prefrontal cortex. Neuroimage *88*, 202–211.

Hutchison, R.M., Gallivan, J.P., Culham, J.C., Gati, J.S., Menon, R.S., and Everling, S. (2012a). Functional connectivity of the frontal eye fields in humans and macaque monkeys investigated with resting-state fMRI. J. Neurophysiol. *107*, 2463–2474.

Hutchison, R.M., Womelsdorf, T., Gati, J.S., Leung, L.S., Menon, R.S., and Everling, S. (2012b). Resting-State Connectivity Identifies Distinct Functional Networks in Macaque Cingulate Cortex. Cereb. Cortex *22*, 1294–1308.

Hutchison, R.M., Womelsdorf, T., Gati, J.S., Everling, S., and Menon, R.S. (2013). Resting-state networks show dynamic functional connectivity in awake humans and anesthetized macaques. Hum. Brain Mapp. *34*, 2154–2177.

Hutchison, R.M., Hutchison, M., Manning, K.Y., Menon, R.S., and Everling, S. (2014). Isoflurane induces dose-dependent alterations in the cortical connectivity profiles and dynamic properties of the brain's functional architecture. Hum. Brain Mapp. *35*, 5754–5775.

Hutchison, R.M., Culham, J.C., Flanagan, J.R., Everling, S., and Gallivan, J.P. (2015). Functional subdivisions of medial parieto-occipital cortex in humans and nonhuman primates using resting-state fMRI. Neuroimage *116*, 10–29.

Laumann, T.O., Gordon, E.M., Adeyemo, B., Snyder, A.Z., Joo, S.J., Chen, M.-Y., Gilmore, A.W., McDermott, K.B., Nelson, S.M., Dosenbach, N.U.F., et al. (2015).

Functional System and Areal Organization of a Highly Sampled Individual Human Brain. Neuron *87*, 657–670.

Leite, F.P., Tsao, D., Vanduffel, W., Fize, D., Sasaki, Y., Wald, L.L., Dale, A.M., Kwong, K.K., Orban, G.A., Rosen, B.R., et al. (2002). Repeated fMRI using iron oxide contrast agent in awake, behaving macaques at 3 Tesla. Neuroimage *16*, 283–294.

Lewis, J.W., and Van Essen, D.C. (2000). Mapping of architectonic subdivisions in the macaque monkey, with emphasis on parieto-occipital cortex. J. Comp. Neurol. *428*, 79–111.

Markov, N.T., Misery, P., Falchier, A., Lamy, C., Vezoli, J., Quilodran, R., Gariel, M.A., Giroud, P., Ercsey-Ravasz, M., Pilaz, L.J., et al. (2010). Weight Consistency Specifies Regularities of Macaque Cortical Networks. Cereb. Cortex *21*, 1254–1272.

Mars, R.B., Jbabdi, S., Sallet, J., O'Reilly, J.X., Croxson, P.L., Olivier, E., Noonan, M.P., Bergmann, C., Mitchell, A.S., Baxter, M.G., et al. (2011). Diffusion-weighted imaging tractography-based parcellation of the human parietal cortex and comparison with human and macaque resting-state functional connectivity. J. Neurosci. *31*, 4087–4100.

Miranda-Dominguez, O., Mills, B.D., Grayson, D., Woodall, A., Grant, K.A., Kroenke, C.D., and Fair, D.A. (2014). Bridging the gap between the human and macaque connectome: a quantitative comparison of global interspecies structure-function relationships and network topology. J. Neurosci. *34*, 5552–5563.

Nelson, E.E., and Winslow, J.T. (2008). Non-Human Primates: Model Animals for Developmental Psychopathology. Neuropsychopharmacology *34*, 90–105.

Neubert, F.-X., Mars, R.B., Sallet, J., and Rushworth, M.F.S. (2015). Connectivity reveals relationship of brain areas for reward-guided learning and decision making in human and monkey frontal cortex. Proc. Natl. Acad. Sci. U. S. A. *112*, E2695–E2704.

O'Connor, D., Potler, N.V., Kovacs, M., Xu, T., Ai, L., Pellman, J., Vanderwal, T., Parra, L., Cohen, S., Ghosh, S., et al. (2016). The Healthy Brain Network Serial Scanning

Initiative: A resource for evaluating inter-individual differences and their reliabilities across scan conditions and sessions.

Paxinos, G., and Franklin, K.B.J. (2004). The Mouse Brain in Stereotaxic Coordinates (Gulf Professional Publishing).

Phillips, K.A., Bales, K.L., Capitanio, J.P., Conley, A., Czoty, P.W., ‘t Hart, B.A., Hopkins, W.D., Hu, S.-L., Miller, L.A., Nader, M.A., et al. (2014). Why Primate Models Matter. Am. J. Primatol. *76*, 801.

Power, J.D., Cohen, A.L., Nelson, S.M., Wig, G.S., Barnes, K.A., Church, J.A., Vogel, A.C., Laumann, T.O., Miezin, F.M., Schlaggar, B.L., et al. (2011). Functional network organization of the human brain. Neuron *72*, 665–678.

Rilling, J.K. Comparative primate neuroimaging: insights into human brain evolution - ScienceDirect.

Schönwiesner, M., Dechent, P., Voit, D., Petkov, C.I., and Krumbholz, K. (2014). Parcellation of Human and Monkey Core Auditory Cortex with fMRI Pattern Classification and Objective Detection of Tonotopic Gradient Reversals. Cereb. Cortex *25*, 3278–3289.

Shen, K., Bezgin, G., Hutchison, R.M., Gati, J.S., Menon, R.S., Everling, S., and McIntosh, A.R. (2012). Information processing architecture of functionally defined clusters in the macaque cortex. J. Neurosci. *32*, 17465–17476.

Vanderwal, T., Eilbott, J., Finn, E.S., Craddock, R.C., Turnbull, A., and Castellanos, F.X. (2017). Individual differences in functional connectivity during naturalistic viewing conditions. Neuroimage.

Vanduffel, W., Zhu, Q., and Orban, G.A. (2014). Monkey cortex through fMRI glasses. Neuron *83*, 533–550.

Van Essen, D.C., Glasser, M.F., Dierker, D.L., and Harwell, J. (2012). Cortical parcellations of the macaque monkey analyzed on surface-based atlases. Cereb. Cortex *22*, 2227–2240.

Vincent, J.L., Patel, G.H., Fox, M.D., Snyder, A.Z., Baker, J.T., Van Essen, D.C., Zempel, J.M., Snyder, L.H., Corbetta, M., and Raichle, M.E. (2007). Intrinsic functional architecture in the anaesthetized monkey brain. Nature *447*, 83–86.

Wang, J., Ren, Y., Hu, X., Nguyen, V.T., Guo, L., Han, J., and Guo, C.C. (2017). Test-retest reliability of functional connectivity networks during naturalistic fMRI paradigms. Hum. Brain Mapp. *38*, 2226–2241.

Wig, G.S., Laumann, T.O., and Petersen, S.E. (2014). An approach for parcellating human cortical areas using resting-state correlations. Neuroimage *93 Pt 2*, 276–291.

Xu, T., Opitz, A., Craddock, R.C., Wright, M.J., Zuo, X.-N., and Milham, M.P. (2016). Assessing Variations in Areal Organization for the Intrinsic Brain: From Fingerprints to Reliability. Cereb. Cortex.

Zuo, X.-N., and Xing, X.-X. (2011). Effects of non-local diffusion on structural MRI preprocessing and default network mapping: statistical comparisons with isotropic/anisotropic diffusion. PLoS One *6*, e26703.

Zuo, X.-N., and Xing, X.-X. (2014). Test-retest reliabilities of resting-state FMRI measurements in human brain functional connectomics: a systems neuroscience perspective. Neurosci. Biobehav. Rev. *45*, 100–118.

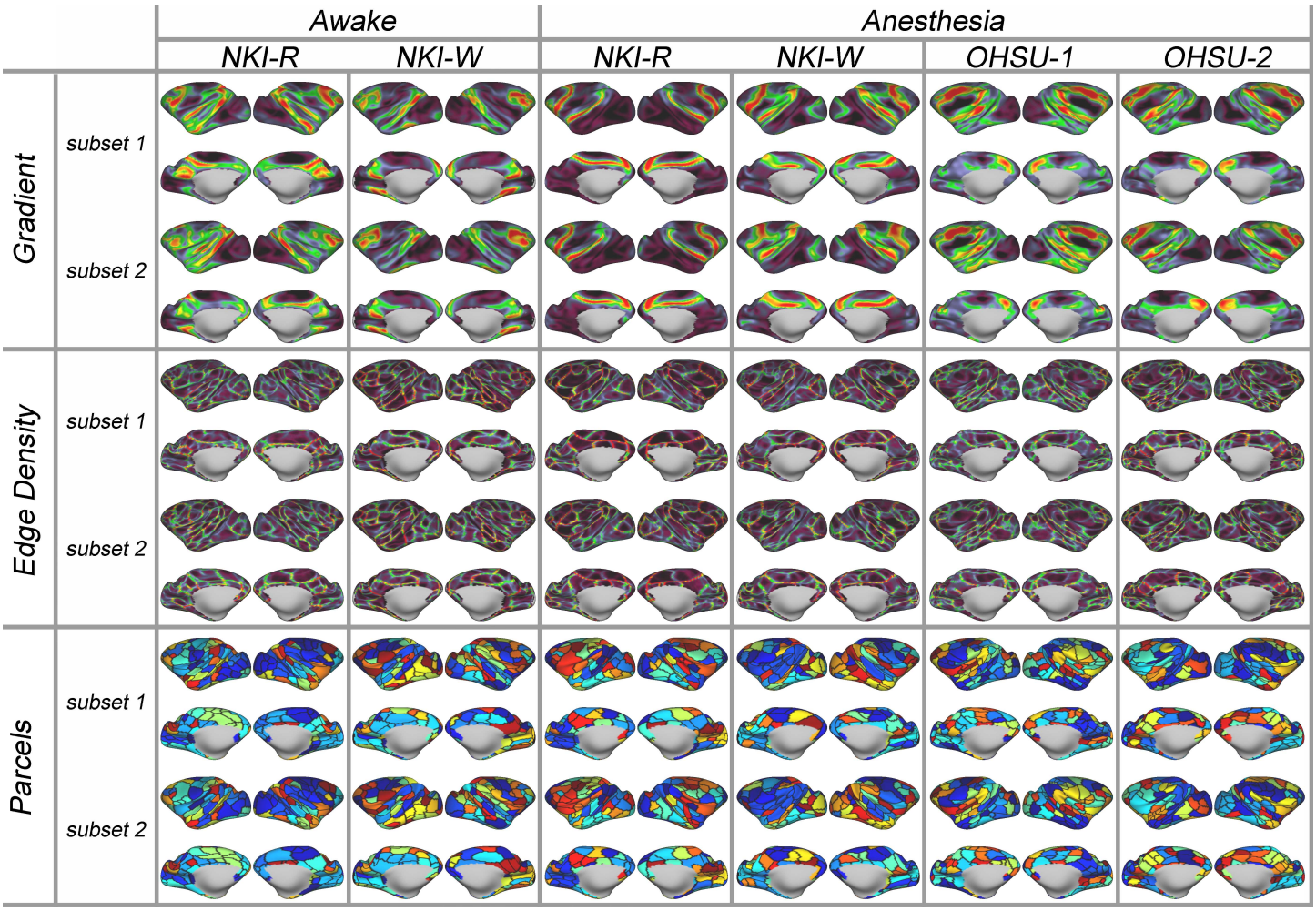
Awake
Anesthesia
NKI-R
NKI-W
NKI-R
NKI-W
OHSU-1
OHSU-2
Gradient
subset 1
subset 2
Edge Density
subset 1
subset 2
Parcels
subset 1
subset 2

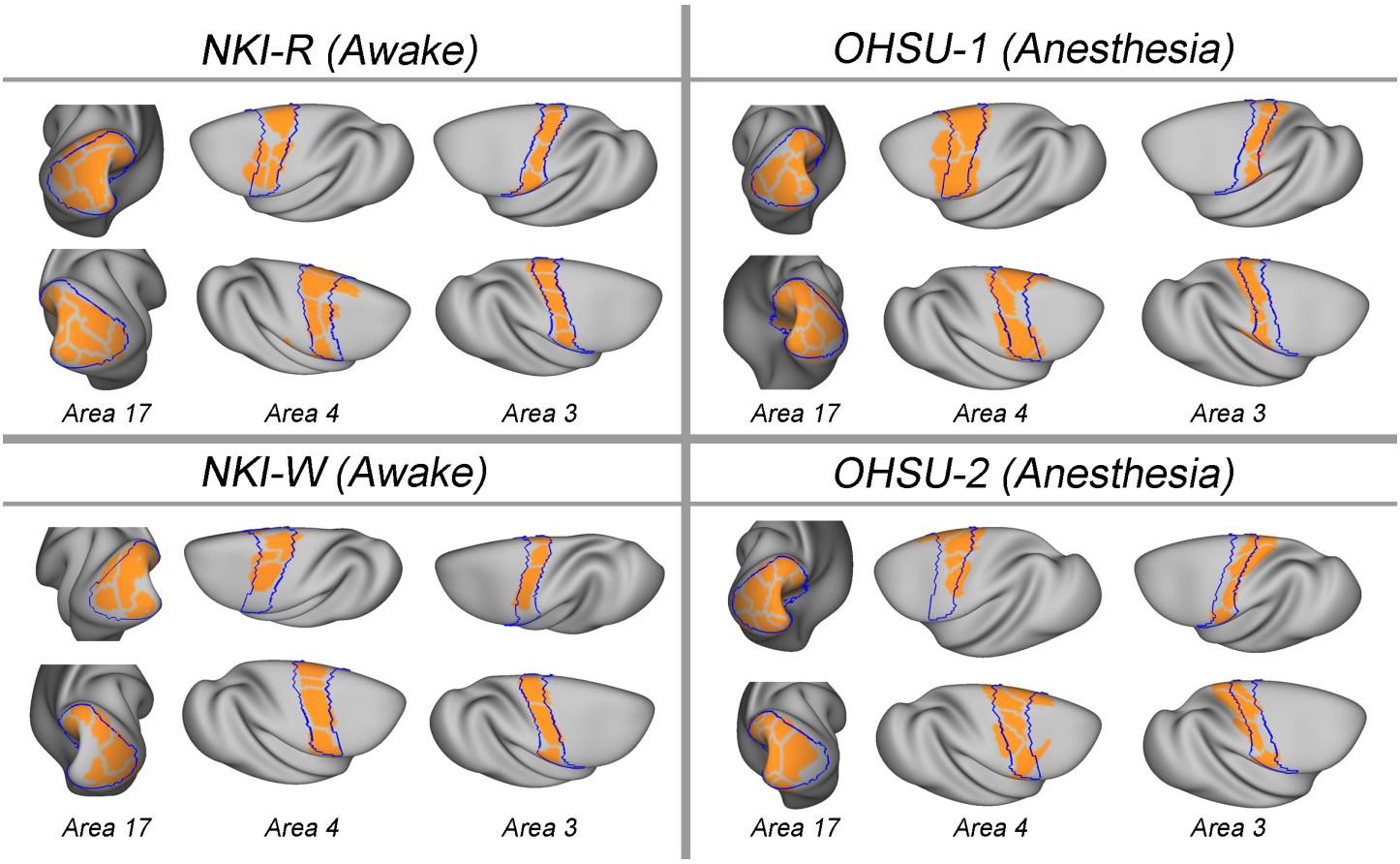
NKI-R (Awake)
OHSU-1 (Anesthesia)
Area 17
Area 4
Area 3
Area 17
Area 4
Area 3
NKI-W (Awake)
OHSU-2 (Anesthesia)
Area 17
Area 4
Area 3
Area 17
Area 4
Area 3

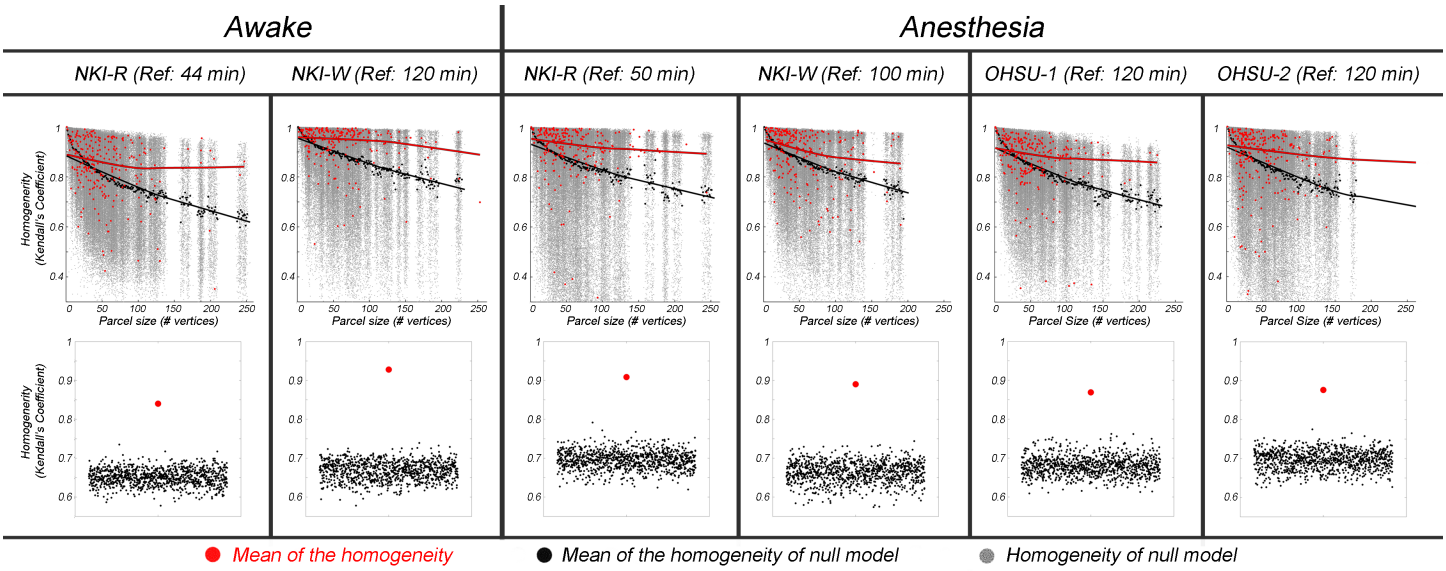
Awake
Anesthesia
NKI-R (Ref: 44 min)
NKI-W (Ref: 120 min)
NKI-R (Ref: 50 min)
NKI-W (Ref: 100 min)
OHSU-1 (Ref: 120 min)
OHSU-2 (Ref: 120 min)
Homogeneity (Kendall's Coefficient)
Parcel size (# vertices)
Parcel Size (# vertices)
Mean of the homogeneity
Mean of the homogeneity of null model
Homogeneity of null model

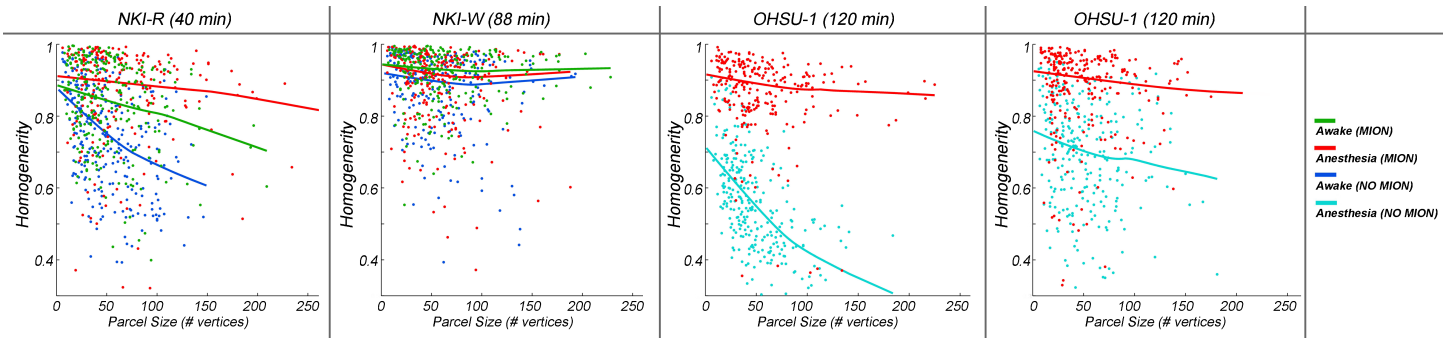
NKI-R (40 min)
NKI-W (88 min)
OHSU-1 (120 min)
OHSU-1 (120 min)
Homogenerity
Parcel Size (# vertices)
Awake (MION)
Anesthesia (MION)
Awake (NO MION)
Anesthesia (NO MION)

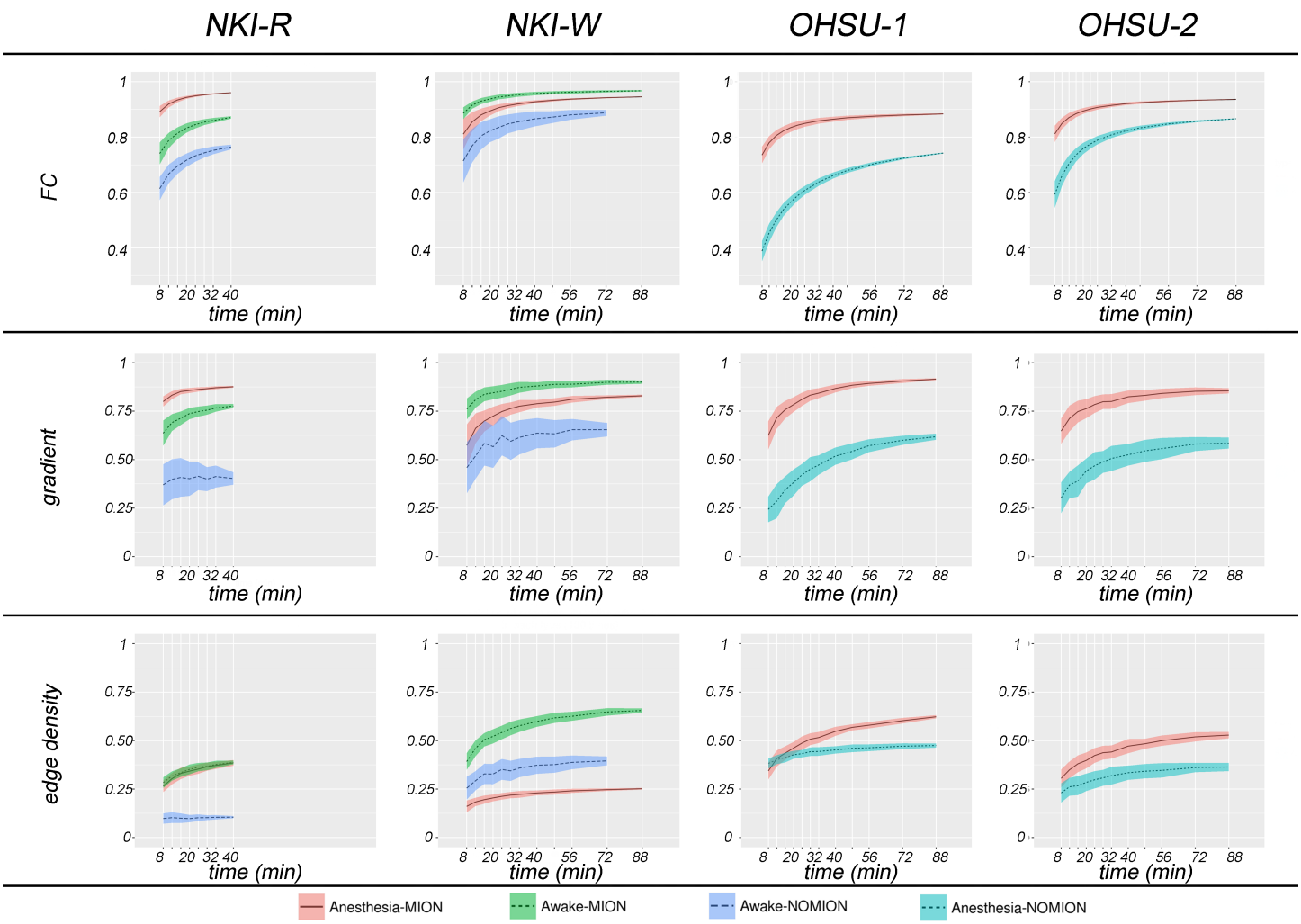
NKI-R
NKI-W
OHSU-1
OHSU-2
FC
gradient
edge density
time (min)
Anesthesia-MION
Awake-MION
Awake-NOMION
Anesthesia-NOMION

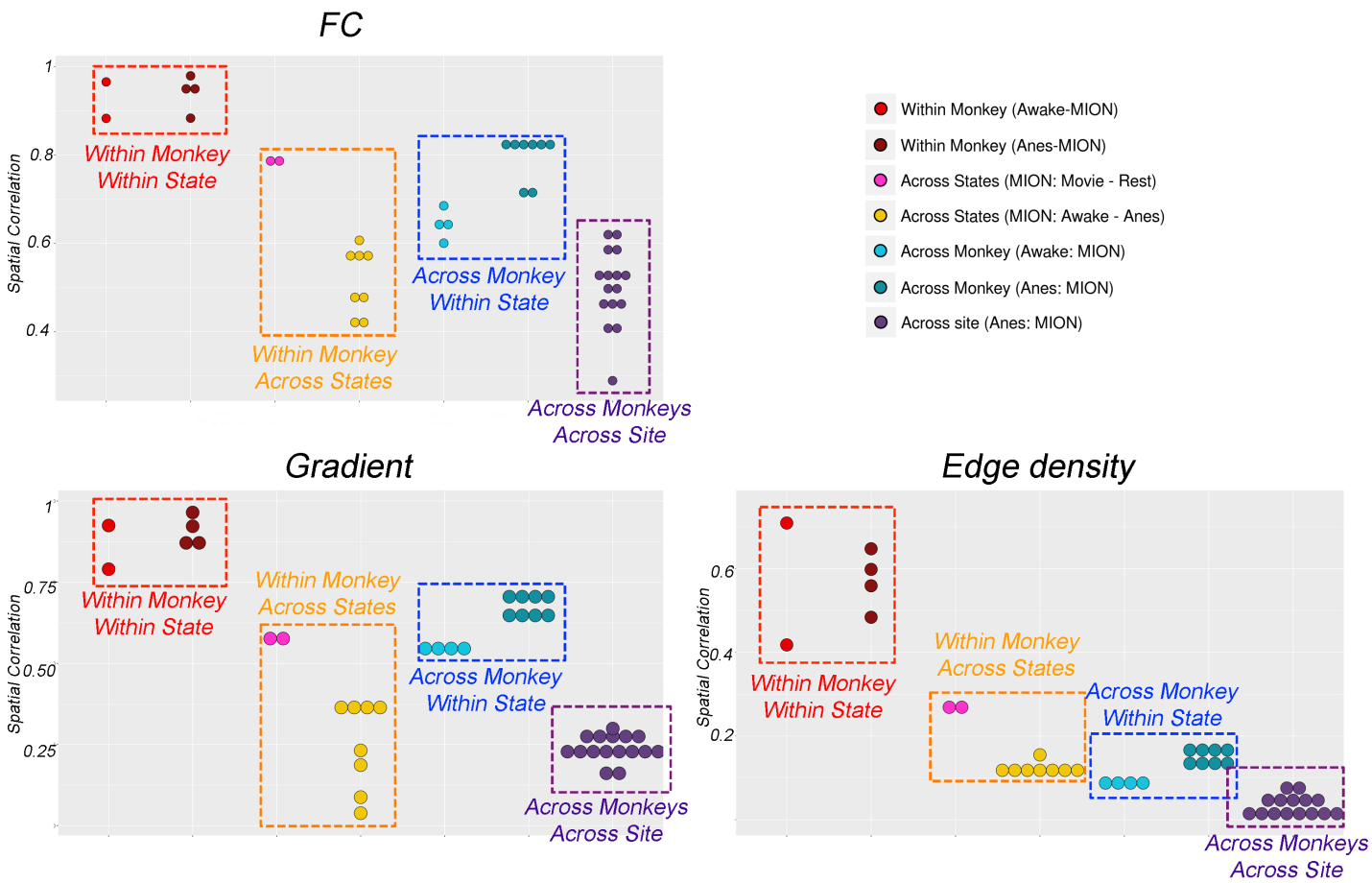
FC
Spatial Correlation
1
0.8
0.6
0.4
Within Monkey
Within State
Within Monkey
Across States
Across Monkey
Within State
Across Monkeys
Across Site
Within Monkey (Awake-MION)
Within Monkey (Anes-MION)
Across States (MION: Movie - Rest)
Across States (MION: Awake - Anes)
Across Monkey (Awake: MION)
Across Monkey (Anes: MION)
Across site (Anes: MION)
Gradient
Spatial Correlation
1
0.75
0.50
0.25
Within Monkey
Within State
Within Monkey
Across States
Across Monkey
Within State
Across Monkeys
Across Site
Edge density
Spatial Correlation
0.6
0.4
0.2
Within Monkey
Within State
Within Monkey
Across States
Across Monkey
Within State
Across Monkeys
Across Site

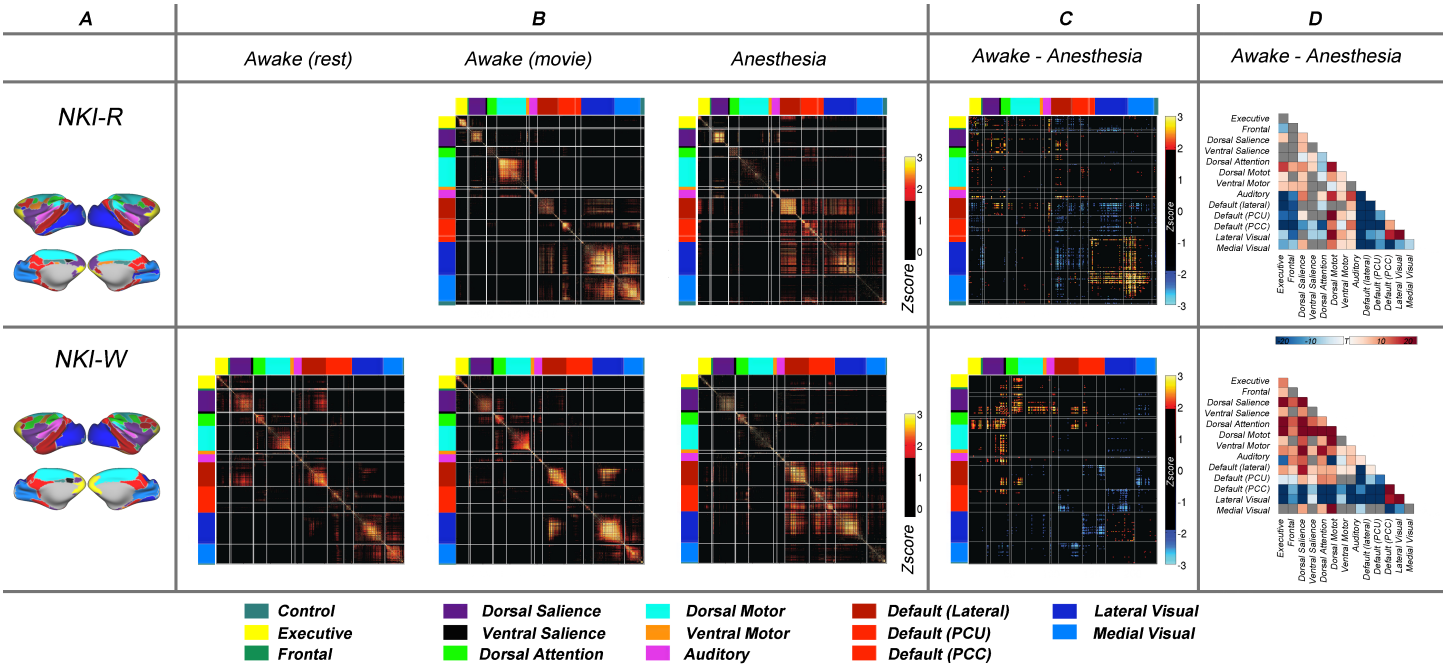
A
B
C
D
Awake (rest)
Awake (movie)
Anesthesia
Awake - Anesthesia
Awake - Anesthesia
NKI-R
NKI-W
Zscore
Executive
Frontal
Dorsal Salience
Ventral Salience
Dorsal Attention
Dorsal Motot
Ventral Motor
Auditory
Default (lateral)
Default (PCU)
Default (PCC)
Lateral Visual
Medial Visual
Control
Executive
Frontal
Dorsal Salience
Ventral Salience
Dorsal Attention
Dorsal Motor
Ventral Motor
Auditory
Default (Lateral)
Default (PCU)
Default (PCC)
Lateral Visual
Medial Visual